

## Electronic structure in the twinned 10M martensite phase of the $\text{Ni}_{49.7}\text{Mn}_{29.1}\text{Ga}_{21.2}$ Heusler alloy: Experiment and theory

Oleg Heczko,\* Václav Drchal, Stanislav Cichoň, Ladislav Fekete, Josef Kudrnovský, Irena Kratochvílová, Ján Lančok, and Vladimír Cháb

*Institute of Physics, the Czech Academy of Sciences, CZ-182 21 Praha 8, Czech Republic*

 (Received 29 June 2018; revised manuscript received 14 September 2018; published 6 November 2018)

In shape memory materials the fine twinned microstructure plays a fundamental role. Here we show that in the martensite phase of Ni-Mn-Ga Heusler alloy, the fine features of electronic structure are not caused by intrinsic electronic changes but mesoscopically different orientations of ferroelastic domains, i.e., twins. The cuts of Fermi surfaces of a (pseudo) tetragonally distorted  $\text{Ni}_{49.7}\text{Mn}_{29.1}\text{Ga}_{21.2}$  Heusler single crystal with a (100) surface orientation were measured using angle-resolved photoemission spectroscopy and compared with first-principles calculations. In this work we demonstrated that the measured photoelectron spectrum was a projection of three separate electronic structures originating from single a-a and two perpendicular a-c ferroelastic domains with a twinned relationship. The twinning results in pseudosplitting of the experimentally observed bands at Fermi level.

DOI: [10.1103/PhysRevB.98.184407](https://doi.org/10.1103/PhysRevB.98.184407)

### I. INTRODUCTION

Despite their discovery more than 100 years ago, Heusler alloys are only now being widely studied for their unique magnetic properties with potential applications in spintronics [1,2] and in search for multiferroic materials [3,4]. These properties are very sensitive to changes in stoichiometry ( $X_2YZ$ ). This high sensitivity provides variability and flexibility for potential use [5]. Moreover, several Heusler alloys exhibit a martensitic transformation, a diffusionless, displacive transformation from the cubic phase (austenite) to a lower-symmetry martensite phase [6]. This transformation is instrumental for baro-, elasto-, and magnetocaloric effects [7–9], and particularly for magnetic shape memory effects [10,11]. However, only a few alloys have exhibited the martensitic transformation in a usable range above room temperature (RT). The best known and most promising and studied examples are off-stoichiometric alloys based on  $\text{Ni}_2\text{MnGa}$  [12–14]. Ni-Mn-Ga martensite exhibits colossal magnetic-field-induced deformation up to 12% due to the magnetically induced reorientation (MIR) of ferroelastic domains in a moderate field below 1 T [15]. Inversely, Ni-Mn-Ga martensite also exhibits a large magnetization change upon mechanical deformation [10,16].

The martensitic transformation to the low-symmetry phase is driven by electronic structure changes [17–19]. To secure elastic compatibility between transforming phases, the martensitic microstructure consists of twinned ferroelastic domains. These coherent domains have different but strictly symmetry-related crystal orientations [4,20] joined by an interface called a twin boundary. In the simplest case of tetragonal martensite, three different orientations of the ferroelastic domains exist in the compound twin relation, i.e., the domains are mirror-symmetry related.

For lower-symmetry phases, several additional modes of twinning exist [20], which provide much more freedom for nucleation and growth of the low-symmetry phase and consequently for the formation of a complex, twinned microstructure of martensite [21]. In Ni-Mn-Ga, the modulated monoclinic structure of martensite, arising from the adaptive behavior [22], results in a complex hierarchical twin microstructure [23].

However, owing to the very small monoclinic deviation from the tetragonal unit cell, the basic structure of Ni-Mn-Ga martensite can be well approximated with a twinned tetragonal crystal structure, i.e., containing only three ferroelastic domains with tetragonal orientations approximately following the cubic axes of original austenite [6,12]. The (pseudo)tetragonal unit cell has approximately the same volume as the cubic cell of austenite with the lattice constant relationship  $c < a$ . This often-used approximation is sufficient for our purposes, as shown later.

Understanding the electronic structure changes upon transformation is key to understanding the origin of the martensitic transformation, a necessary condition to obtain shape memory, caloric, and multiferroic effects. Theoretical studies of the  $\text{Ni}_2\text{MnGa}$  alloy indicate possible band splitting, namely, a spin-split band has been predicted by varying the magnetization value in the premartensitic phase [24]. On the other hand, emerging modulation of the premartensitic phase in  $\text{Ni}_2\text{MnGa}$  is ascribed to the existence of a Kohn anomaly in cubic austenite [25]. This was further supported by experimental investigation of the Fermi surface of cubic  $\text{Ni}_2\text{MnGa}$  using positron annihilation [26].

In  $\text{Ni}_2\text{Mn}_{1+x}\text{Sn}_{1-x}$  alloys [27], the interaction of Ni  $3d$  and Mn  $3d$  electrons were found to be important, as these interactions influence the states in the vicinity of the Fermi level,  $E_F$ . The connection between the electronic structure and ferromagnetism in the transforming Heusler alloy is summarized in Ref. [17], providing an understanding of the

\*Corresponding author: heczko@fzu.cz

Jahn-Teller splitting of  $E_F$  at the M-A phase transition. This type of interaction produces band splitting in several bonding and antibonding states that cross  $E_F$ . However, none of the published works considered the twinned microstructure of the martensitic phase and the complex magnetic domain structure arising from different orientations and arrangements of ferroelastic domains.

Photoemission (PE) has been commonly applied to study the electronic structure or local arrangement of atoms and their chemistry since the 1960s [28]. The capability of the electron dispersion relations  $E$  vs  $k$  mapping is substantially enhanced with the application of photoelectron emission microscopy (PEEM). Moreover, switching between real space and diffraction imaging modes of the microscope can be successfully used to directly study the electronic structure connected to a selected object on a sample surface [29,30].

Recently, we used angle-resolved ultraviolet photoelectron spectroscopy (ARUPS) to reveal the electronic structure of the cubic austenitic phase of the  $\text{Ni}_{49.7}\text{Mn}_{29.1}\text{Ga}_{21.2}(100)$  Heusler alloy [31]. Our theoretical calculations of the spectra using the coherent potential approximation (CPA) approximation agreed well with the experimental data, namely, the spectra close to  $E_F$ . However, the experimentally determined electronic structure was found to be gradually smeared below 1 eV due to a significant disorder effect which was much stronger than predicted by theoretical simulations.

In this work, we relate the experimental ARUPS spectra and microstructure of  $\text{Ni}_{49.7}\text{Mn}_{29.1}\text{Ga}_{21.2}(100)$  martensite to theoretical simulations, including consideration of disorder effects. We found a considerable change of the electronic structure at  $E_F$  caused by the austenite-martensite phase transition, and the observed bands were split. We show that an assumed tetragonal distortion can explain the ARUPS features observed in martensite.

## II. MATERIALS AND METHODS

We used single-crystal  $\text{Ni}_{49.7}\text{Mn}_{29.1}\text{Ga}_{21.2}$  with a transformation temperature to martensite above RT. The crystal exhibits magnetic-induced reorientation at RT in magnetic field below 1 T. The structure of martensite is a modulated 10M structure with a monoclinic unit cell, which can be well approximated as a (pseudo)tetragonal structure with  $c = 0.565$  nm and  $a = 0.596$  nm at room temperature. The short axis, i.e.,  $c$  axis, is an easy axis of magnetization. The crystal was cut along the (100) plane of austenite with precision of a few degrees. The sample was electropolished, and then the clean sample surface was prepared for ultrahigh vacuum (UHV) by cycles of  $\text{Ar}^+$  sputtering and subsequent annealing at 400 °C. The martensite (100) and (001) planes deviate from the surface plane by a few degrees, as determined by the geometry of transformation [20,23]. The PEEM and magnetic force microscopy (MFM) measurements were performed at RT, and the detailed description of the experimental conditions is given in Ref. [32].

The electronic structure of disordered  $\text{Ni}_2\text{Mn}_{1.16}\text{Ga}_{0.84}$  alloy in the ferromagnetic tetragonal (martensitic) phase with  $c/a = 0.94$  was calculated using the scalar-relativistic tight-binding linear muffin-tin orbital (TB-LMTO) method [33,34] and the local density approximation. The effect of

disorder was included within the CPA [34]. The disordered  $\text{Ni}_2\text{Mn}_{1.16}\text{Ga}_{0.84}$  model alloy closely corresponds to chemical composition in the experiment. The disordered phase is Mn-rich with extra Mn atoms distributed randomly on the Ga sublattice and spins oriented antiparallel to Mn spins on the Mn sublattice. We used the *spd* basis, the experimental lattice constants  $a = 5.4755$  Å,  $c = 6.0080$  Å, 280  $k$  points in the irreducible wedge of the Brillouin zone, and the Vosko-Wilk-Nusair exchange-correlation potential [35]. The calculations were performed at 0 K. Some qualitative features of the electronic structure should be mentioned: (i) The effect of disorder depends on the  $k$  vector and on the energy. Features moving with the  $k$  vector are band-structure-like, while those independent of the  $k$  vector correspond to quasilocalized states due to disorder. (ii) Most states in the energy regions of interest, with binding energies around  $-1$  eV and in the interval  $(-4, -3)$  eV, come mostly from Ni states. Spectral densities are modified by the many-body effects that influence both the final and the initial (valence) states and are energy- and  $k$ -vector sensitive. Contrary to the effect of disorder, the states directly at  $E_F$  are only shifted but not damped, and the damping increases with the binding energy.

The ARUPS intensity was calculated in the same way as in our study of the  $\text{Ni}_2\text{MnGa}$  alloy in the austenite phase [31]. We approximated the semi-infinite solid by a bulk phase, employed the approximation of a constant matrix element, and neglected the final state effects. The alloy randomness was included via the CPA. Thus the information on the electronic structure and Bloch spectral density is contained in the configurationally averaged Green function. Instead of the Brillouin zone (BZ), we used a prismatic zone with the same volume as the BZ, and its repetition covers the entire reciprocal space. The  $k$  vector is decomposed into its parallel  $k_{\parallel}$  (with the surface) and perpendicular  $k_z$  parts. We divided the basal plane of the prismatic zone into small rectangles with sides equal to  $2\pi / (80a)$  or  $2\pi / (80c)$  that define the  $k$ -space sampling.

A NanoESCA photoemission spectrometer (Oxford Instruments Omicron NanoScience) based on a PEEM column and a double-hemispherical-imaging energy filter was used. The basic pressure in the analytical chamber was lower than  $10^{-10}$  Torr. The surface quality was monitored by low-energy electron diffraction (LEED) and the electron spectroscopy for chemical analysis (ESCA) mode. The PEEM microscope operating in diffraction mode was used to acquire the equi-energetic cuts through the first BZ using a He-I discharge lamp. The energy resolution was 0.1 eV, and the equi-energy cuts through the  $k$  space were performed with 0.05-eV steps in the interval of  $(E_F - 3, E_F)$  eV.

## III. RESULTS AND DISCUSSION

After UHV cleaning and annealing at 670 K, the phase transformation from cubic austenite to martensite occurred during cooling at approximately 305 K. The transformation resulted in spontaneously twinned martensite with ferroelastic domains of different orientations and different thicknesses. A selected MFM image of the striped twin microstructure on the (001) surface face is shown in Fig. 1, visualizing the arrangement of magnetic domains in differently oriented ferroelastic domains connected by an a-c twin plane.

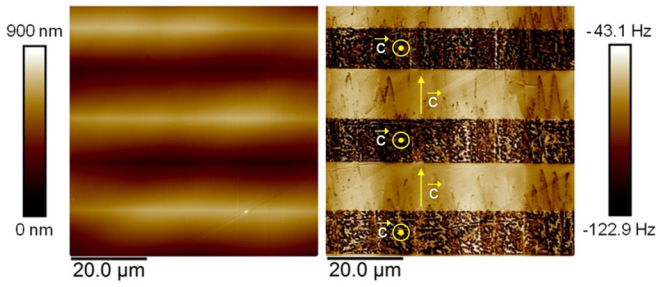


FIG. 1. AFM/MFM images of the (001) surface of the  $\text{Ni}_{49.7}\text{Mn}_{29.1}\text{Ga}_{21.2}(100)$  single crystal in the martensitic phase. The twinned microstructure of the ferroelastic domains is visible as surface relief in the topographic AFM image (left). MFM image of the magnetic domains of the individual a-a and a-c ferroelastic domains (right). The orientation of the  $c$  axis, identified as the easy direction of magnetization, is marked on the MFM image.

Considering the (pseudo)tetragonal lattice with the magnetization easy axis along the  $c$  axis, the observed labyrinth domains indicate that the magnetization (i.e.,  $c$  axis) is perpendicular to the surface, and the dagger domains indicate that the magnetization ( $c$  axis) is approximately in the surface plane perpendicular to the twin plane. The detailed analysis of the stripes [32] confirmed the a-c twinning [23]. The observed magnetic domain structure indicates that the surface contains two differently oriented ferroelastic domains on the mezo- or microscopic scales. These domains will be further referred to as a-a domain ( $c$  axis perpendicular to the surface) or a-c domain ( $a$  axis perpendicular to the surface). Moreover, the a-c domains can have two orientations with the  $c$  axes perpendicular to each other. The analyzed martensitic single crystal is thus a complex object reflecting a particular structural and magnetic orientation due to twinning. This can be a significant source of spectral distortion in addition to the disorder caused by the off-stoichiometry and magnetic disorder in the finite temperature. Although the presence of ferroelastic and ferromagnetic interfaces violates  $k$ -vector conservation during the scattering process of forming the photoelectron spectra, the main features in the ARUPS spectra are still well defined.

The experimental ARUPS results from large sample areas are summarized in Fig. 2. The equi-energetic cuts through the three-dimensional BZ demonstrate the valence-band features of the  $\text{Ni}_{49.7}\text{Mn}_{29.1}\text{Ga}_{21.2}(100)$  oriented single crystal in the martensitic phase. The images taken below  $E_F$  indicate the mirrorlike symmetry of the cuts through the full range of measured energies, i.e.,  $(E_F - 3, E_F)$  eV. However, at lower energies, the symmetry becomes slightly distorted. The images acquired around  $E_F$  exhibit well-resolved band splitting into two subbands. At approximately  $-1$  eV, the splitting is eliminated and replaced with four symmetric squarelike spots. At  $-2$  eV, these spots are substituted with a moderately distorted four-pointed star. These particular binding energies are significant, as they cluster the snapshots of the BZ cut into three groups with very similar spectra which suddenly change at these energies. In each particular group, the snapshots keep the shape and basic parameters independent of the binding energy within the interval (Fig. 2). These abrupt changes in the characteristics of the spectra are quite unusual and indicate the high degree of localization in the  $k_z$  direction.

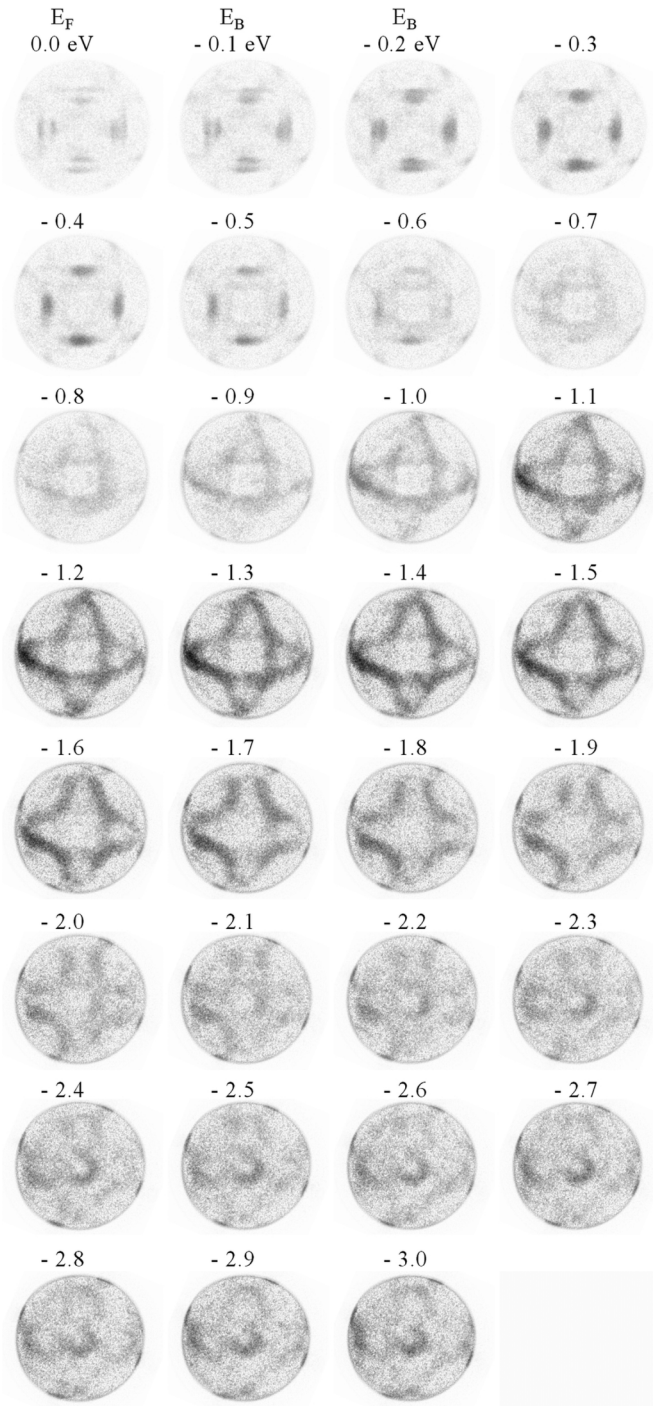


FIG. 2. Sequence of PEEM images of equi-energetic cuts through the first Brillouin zone (BZ) of martensite in the energy range from  $-3$  eV to  $E_F$ . High intensity is dark. The images cover the entire first BZ.

Detailed large-area images acquired at  $E_F$  of martensite, austenite, and their difference are shown in comparison in Fig. 3. The martensite image exhibits two well-resolved essential features: (i) full mirror symmetry and (ii) splitting of the bands at  $E_F$  into two subbands. The difference process, i.e., subtraction of the spectrum of cubic austenite, removes the band splitting seen in the ARUPS equi-energetic cut at  $E_F$  of the martensite phase. The resulting feature corresponds

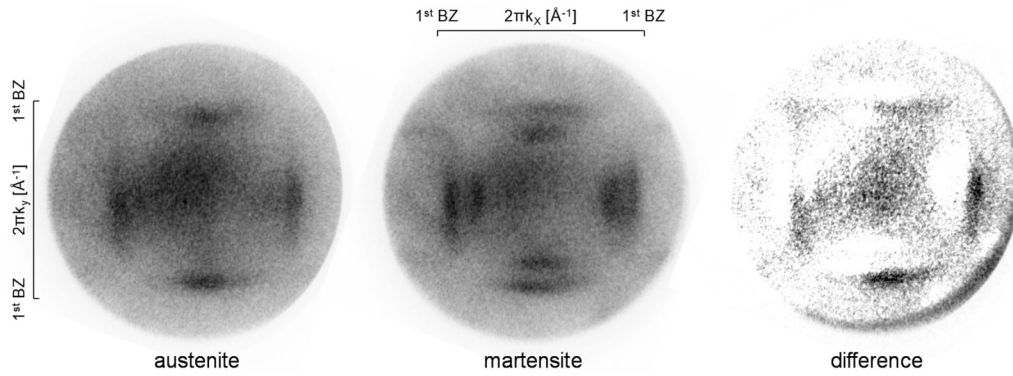


FIG. 3. PEEM images of an equi-energetic cut at  $E_F$  of martensite and austenite and their difference. High intensity is dark. The images cover the entire first BZ, as indicated.

with a single domain structure similar to the image given in Fig. 4. Comparing  $a_M$  and  $c_M$  lattice constants of martensitic phase, the a-a distance reads a bigger value than the c-c one. A similar value of the  $a_A$  and  $a_M$  lattice constants in both phases produces an extinction of their features in the equi-energetic cuts, and the remaining characteristics in the difference image are associated with the c-c distance in the  $k$  space of martensite. It is apparent that there is no splitting in the bands for this artificial c-c case.

Importantly, we were also able to find a few-square-micrometer area where only a single a-a ferroelastic domain of martensite was present. Using the ultimate resolution of the PEEM microscope, we obtained a different ARUPS image at the  $E_F$ . It is shown in Fig. 4. Although the image still shows mirror symmetry, in contrast to the previous ARUPS image at the  $E_F$  shown in Fig. 2, the cut from this area exhibits *no* splitting. Due to the small illuminated area, the quality of the image is rather low with some ghost traits; however, the basic features are well recognized. We can conclude that a single twin variant, i.e., the domain with single-crystal orientation, does not exhibit any band splitting.

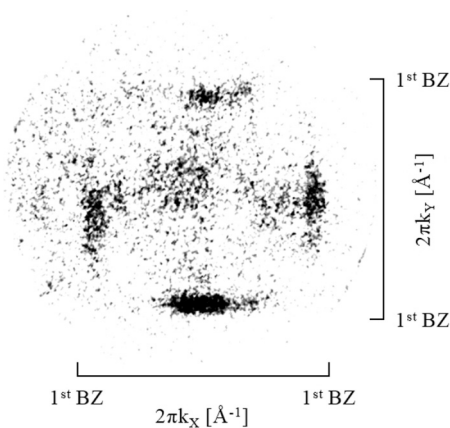


FIG. 4. PEEM image of an equi-energetic cut at  $E_F$  of martensite acquired from the single a-a domain. High intensity is dark. The image covers the entire first BZ, as indicated. In fact, the image copies the structure of the cut obtained in the austenitic phase presented in Fig. 3.

To understand this behavior, a theoretical simulation was performed using the crystallographic structure of the  $\text{Ni}_2\text{MnGa}$  Heusler alloy *including* tetragonal distortion with a primitive cell composed of three atomic layers. The full set of  $k_x$ ,  $k_y$ , and  $k_z$  vectors was applied to calculate the ARUPS spectra projected on a hemispherical cut at a particular  $E_B$ , and the details of this simulation are published in Ref. [31]. The cuts at  $E_B = E_F$  are drawn separately for the a-a and c-a ferroelastic domains at the (100) face of the crystal and are displayed in Fig. 5 (left) and Fig. 5 (middle), respectively. The spectra in these cuts through the first BZ exhibit one substantial difference compared with the full set of experimental data shown in Fig. 2. There is no band splitting and the symmetry is only correlated to the differently oriented structural variations.

Comparing Fig. 2 at  $E_F$  and Fig. 5 (left and middle), the as-measured electronic structure of the sample in the martensitic phase does not possess similarity to the theoretically predicted band structure of the  $\text{Ni}_{49.7}\text{Mn}_{29.1}\text{Ga}_{21.2}(100)$  single crystal in any considerable symmetry direction of the BZ. However, the simulated spectrum agrees with the experimental data measured solely in a single a-a domain (Fig. 4) where no band splitting and no symmetry breakdown were observed (Fig. 5, left).

Generally, it is not valid for a spontaneously transformed sample, since such a sample contains many twinned variants of all three orientations. Any comparison between theoretical calculation and experiment must consider that the instrument summarizes all contributions from the illuminated surface, and the ARUPS spectrum is composed of the  $E_F$  spectra from all the ferroelastic domain orientations, i.e., from the a-a and two c-a domains.

Figure 5 (right) represents a new simulated spectrum obtained simply by summation of the spectra originating from the a-a and two a-c domains (Fig. 5, left and middle). The a-a configuration was used as a base spectrum, and the two a-c configurations were added with the  $c$  axis perpendicular to each other. Such a composed spectrum reproduces all features characteristic of the electronic structure at  $E_F$  experimentally found, and only this combination of all three simulated variants at  $E_F$  provides good agreement with the measured spectrum. This, we believe, is the origin of the observed splitting and symmetry breakdown in the narrow energy interval below  $E_F$ .

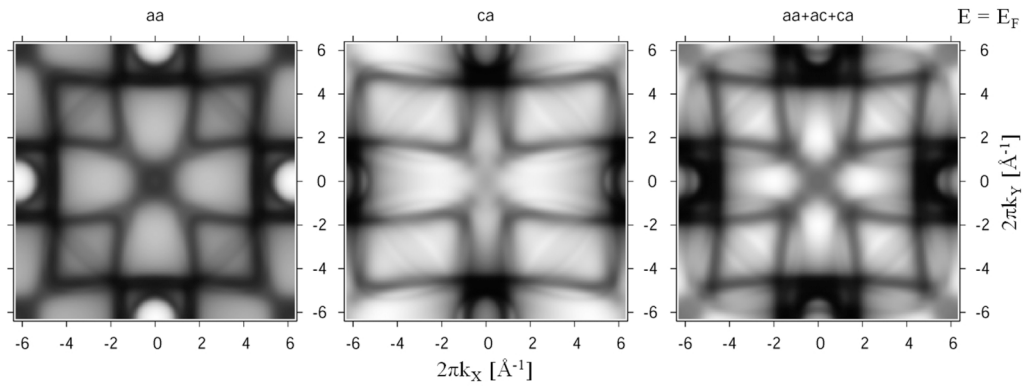


FIG. 5. Theoretical ARUPS images of martensite of the first BZ. High intensity is dark. Left: Single ferroelastic domain with the crystal surface parallel to the tetragonal axes  $a$ , i.e.,  $c$  axis perpendicular to the surface (denoted as a-a). Middle: Single ferroelastic domain with the crystal surface parallel to the tetragonal axes  $a$  and  $c$ , i.e.,  $a$  axis perpendicular to the surface (denoted as c-a). Right: Composed image of the superposition of the a-a, a-c, and c-a domains present in twinned martensite (denoted as aa+ac+ca).

Direct comparison of the theoretical and measured cut of the Fermi surface is provided in Fig. 6. Predicted splitting quite agrees with the measured one. The experimental intensi-

ties depend on twin variant distribution, i.e., on the contribution of each variant orientation. The distribution is established randomly after spontaneous transformation to martensite to

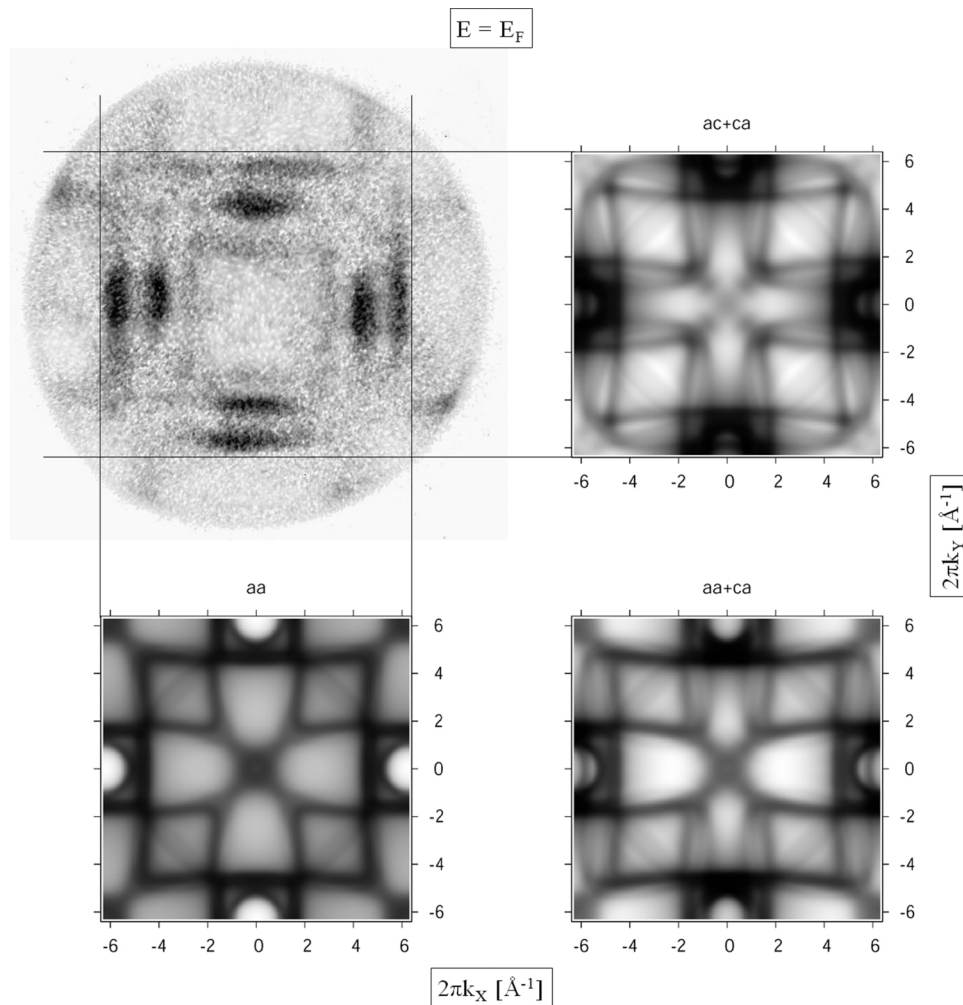


FIG. 6. Comparison of measured (upper left) and theoretical (upper right, bottom left, and bottom right) cut of a twinned martensite Fermi surface. High intensity is dark. Right images: composed theoretical images of the superposition of the a-c plus c-a (up) and a-a plus c-a (bottom) domains present in twinned martensite. For the sake of clarity the comparison is done for the a-a variant and a summation of two a-c and c-a variants.

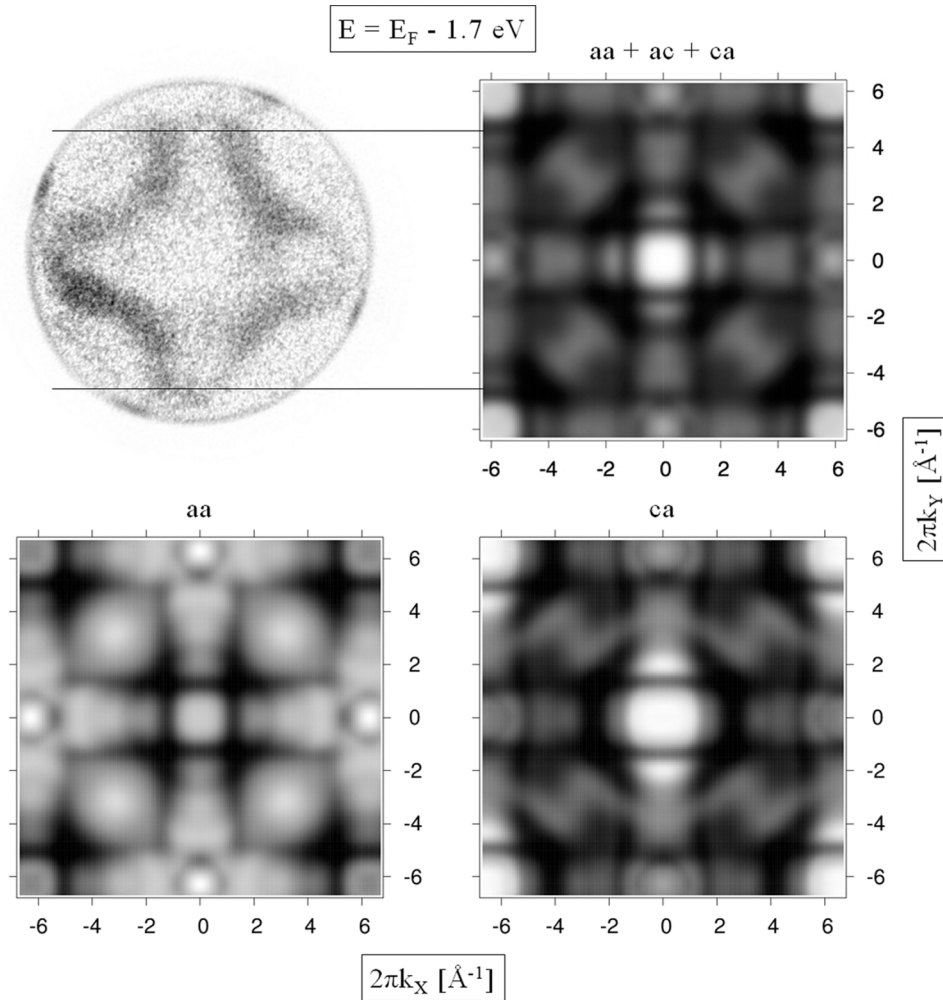


FIG. 7. Comparison of measured (upper left) and theoretical (upper right, bottom left, and bottom right) cut of a twinned martensite Fermi surface 1.7 eV below Fermi energy  $E_F$ . High intensity is dark. Right top: Composed theoretical images of the superposition of the a-c, c-a, and a-c domains present in twinned martensite. Bottom: Theoretical images originating from individual a-a and c-a domains.

secure the compatibility. Although one can expect that volume ratio between variants is equal, it is well known that this is not necessarily the case and some variants can dominate the transformation [20,36]. Thus the experimental intensities can be skewed.

The observed splitting gradually vanishes below Fermi energy, and the entire character of the Fermi surface cut changes (Fig. 2). A detailed comparison of experimental measurement and theoretical calculation for energy 1.7 eV below Fermi energy is presented in Fig. 7. Due to the high disorder, which increases below  $E_F$  as discussed in [31], only strong four-symmetrical crescentlike features are identifiable, both in the theoretical and experimental pictures, and overall symmetry is kept. There is no splitting, either in the theoretical or experimental cut.

Apart from splitting due to the twinned microstructure and spectra smearing ascribed to magnetic and compositional disorder (presented even in austenite) [31], we observed an additional effect very apparent by comparing Figs. 2 and 4 and the theoretical spectra in Fig. 5. In the spectrum taken from twinned martensite (Fig. 2), an apparent hollow space in

the vicinity of the  $\Gamma$  point (center of the figure) is observed, which is in contrast to the spectrum measured from a single domain (Fig. 4) and the theoretical spectrum which exhibits a non-negligible intensity in the center region. The illuminated surface consists of twinned ferroelastic domains with different crystallographic and magnetization orientations. In other words, a high concentration of magnetic domain walls and ferroelastic domain interfaces or twin planes exist. Moreover, the magnetic domains branch on the surface, and their structure mimics a quasifractal stage [37,38], increasing the density of the boundaries near the surface. Based on Snell's law, the electrons with a  $k$  vector close to the  $\Gamma$  point are filtered out on these interfaces and do not contribute to the measured spectra. In a single a-c domain, this effect is negligible, as no twin boundaries and only a few magnetic domains exist, as inferred from Fig. 1.

#### IV. CONCLUSIONS

ARUPS measurements using PEEM combined with theoretical simulations of the equi-energetic cuts through the first

BZ were successfully applied to map the electronic structure in an off-stoichiometric  $\text{Ni}_{49.7}\text{Mn}_{29.1}\text{Ga}_{21.2}(100)$  single-crystal Heusler alloy. We demonstrated that in the martensite phase of Ni-Mn-Ga Heusler alloy, the splitting in the electronic structure observed at  $E_F$  is not caused by intrinsic electronic changes but mesoscopically different orientations of ferroelastic domains. The measured photoelectron spectrum was shown to be a projection of three separate electronic structures originating in a-a and two perpendicular a-c twinned ferroelastic variants, which results in pseudosplitting of the experimentally observed bands at  $E_F$ . Our work thus demonstrates that, in the twinned low-symmetry phase of Ni-Mn-Ga Heusler alloy, not only the atomistic structure but also the fine twinned microstructure at mesoscopic level must be considered to properly un-

derstand the electronic and physical properties of such a material.

#### ACKNOWLEDGMENTS

This work was supported by the Czech Science Foundation through Projects No. 17-19910Y (S.C.) and No. 17-00062S (O.H.) and in part by the Operational Programme Research, Development and Education, financed by the European Structural and Investment Funds and the Czech Ministry of Education, Youth and Sports through Project No. SOLID21 – CZ.02.1.01/0.0/0.0/16\_019/0000760). We further thank the Ministry of Education, Youth and Sports of the Czech Republic (Projects No. LM2015088 and No. LO1409) for infrastructure support.

- 
- [1] T. Jungwirth, X. Marti, P. Wadley, and J. Wunderlich, *Nat. Nanotechnol.* **11**, 231 (2016).
- [2] S. Chadov, X. L. Qi, J. Kubler, G. H. Fecher, C. Felser, and S. C. Zhang, *Nat. Mater.* **9**, 541 (2010).
- [3] A. K. Nayak, V. Kumar, T. Ma, P. Werner, E. Pippel, R. Sahoo, F. Damay, U. K. Rossler, C. Felser, and S. S. P. Parkin, *Nature (London)* **548**, 561 (2017).
- [4] Y. Ganor, T. Dumitrica, F. Feng, and R. D. James, *Philos. Trans. R. Soc., A* **374**, 20150208 (2016).
- [5] T. Graf, C. Felser, and S. S. P. Parkin, *Prog. Solid State Chem.* **39**, 1 (2011).
- [6] P. J. Webster, K. R. A. Ziebeck, S. L. Town, and M. S. Peak, *Philos. Mag. B* **49**, 295 (1984).
- [7] L. Manosa, D. Gonzalez-Alonso, A. Planes, E. Bonnot, M. Barrio, J. L. Tamarit, S. Aksoy, and M. Acet, *Nat. Mater.* **9**, 478 (2010).
- [8] E. Bonnot, R. Romero, L. Manosa, E. Vives, and A. Planes, *Phys. Rev. Lett.* **100**, 125901 (2008).
- [9] J. Liu, T. Gottschall, K. P. Skokov, J. D. Moore, and O. Gutfleisch, *Nat. Mater.* **11**, 620 (2012).
- [10] K. Ullakko, J. K. Huang, C. Kantner, R. C. O’Handley, and V. V. Kokorin, *Appl. Phys. Lett.* **69**, 1966 (1996).
- [11] R. Kainuma, Y. Imano, W. Ito, Y. Sutou, H. Morito, S. Okamoto, O. Kitakami, K. Oikawa, A. Fujita, T. Kanomata, and K. Ishida, *Nature (London)* **439**, 957 (2006).
- [12] O. Heczko, N. Scheerbaum, and O. Gutfleisch, Magnetic shape memory phenomena, in *Nanoscale Magnetic Materials and Applications*, edited by J. P. Liu, E. Fullerton, and O. Gutfleisch (Springer Science Business Media, Boston, MA, 2009).
- [13] M. Thomas, O. Heczko, J. Buschbeck, U. K. Rossler, J. McCord, N. Scheerbaum, L. Schultz, and S. Fahler, *New J. Phys.* **10**, 023040 (2008).
- [14] D. C. Dunand and P. Mullner, *Adv. Mater.* **23**, 216 (2011).
- [15] A. Sozinov, A. A. Likhachev, N. Lanska, and K. Ullakko, *Appl. Phys. Lett.* **80**, 1746 (2002).
- [16] L. Straka, A. Soroka, O. Heczko, H. Hanninen, and A. Sozinov, *Scr. Mater.* **87**, 25 (2014).
- [17] P. Entel, V. D. Buchelnikov, M. E. Gruner, A. Hucht, V. V. Khovailo, and S. K. Nayak, A summary of recent achievements, in *Advances in Shape Memory Materials: Magnetic Shape Memory Alloys*, edited by V. A. Chernenko (Trans Tech, Stafa-Zuerich, 2008).
- [18] R. Niemann, U. K. Rossler, M. E. Gruner, O. Heczko, L. Schultz, and S. Fahler, *Adv. Eng. Mater.* **14**, 562 (2012).
- [19] P. J. Brown, A. Y. Bargawi, J. Crangle, K. U. Neumann, and K. R. A. Ziebeck, *J. Phys.: Condens. Matter* **11**, 4715 (1999).
- [20] K. Bhattacharya, *Microstructure of Martensite: Why It Forms and How It Gives Rise to the Shape-Memory Effect?* (Oxford University Press, Oxford, 2012).
- [21] Y. Song, X. Chen, V. Dabade, T. W. Shield, and R. D. James, *Nature (London)* **502**, 85 (2013).
- [22] S. Kaufmann, U. K. Rossler, O. Heczko, M. Wuttig, J. Buschbeck, L. Schultz, and S. Fahler, *Phys. Rev. Lett.* **104**, 145702 (2010).
- [23] O. Heczko, L. Straka, and H. Seiner, *Acta Mater.* **61**, 622 (2013).
- [24] Y. Lee, J. Y. Rhee, and B. N. Harmon, *Phys. Rev. B* **66**, 054424 (2002).
- [25] C. Bungaro, K. M. Rabe, and A. Dal Corso, *Phys. Rev. B* **68**, 134104 (2003).
- [26] T. D. Haynes, R. J. Watts, J. Laverock, Z. Major, M. A. Alam, J. W. Taylor, J. A. Duffy, and S. B. Dugdale, *New J. Phys.* **14**, 035020 (2012).
- [27] T. Krenke, M. Acet, E. F. Wassermann, X. Moya, L. Manosa, and A. Planes, *Phys. Rev. B* **72**, 014412 (2005).
- [28] F. J. Himpsel, *Appl. Opt.* **19**, 3964 (1980).
- [29] X. Gao, A. N. Koveshnikov, R. H. Madjoe, R. L. Stockbauer, and R. L. Kurtz, *Phys. Rev. Lett.* **90**, 037603 (2003).
- [30] M. Kotsugi, W. Kuch, F. Offi, L. I. Chelaru, and J. Kirschner, *Rev. Sci. Instrum.* **74**, 2754 (2003).
- [31] Y. Polyak, V. Drchal, J. Kudrnovsky, O. Heczko, J. Honolka, V. Chab, J. Kopecek, and J. Lancok, *Phys. Rev. B* **91**, 165115 (2015).
- [32] K. Horakova, V. Chab, O. Heczko, V. Drchal, L. Fekete, J. Honolka, J. Kopecek, J. Kudrnovsky, Y. Polyak, P. Sajdl, M. Vondracek, J. Lancok, V. Feyer, C. Wiemann, and C. M. Schneider, *J. Appl. Phys.* **120**, 113905 (2016).
- [33] O. K. Andersen and O. Jepsen, *Phys. Rev. Lett.* **53**, 2571 (1984).

- [34] I. Turek, V. Drchal, J. Kudrnovsky, M. Sob, and P. Weinberger, *Electronic Structure of Disordered Alloys, Surfaces and Interfaces* (Springer US, New York, 1997).
- [35] S. H. Vosko, L. Wilk, and M. Nusair, *Can. J. Phys.* **58**, 1200 (1980).
- [36] L. Straka, O. Heczko, and H. Hänninen, *Acta Mater.* **56**, 5492 (2008).
- [37] O. Heczko, V. Kopecký, L. Fekete, K. Jurek, J. Kopeček, L. Straka, and H. Seiner, *IEEE Trans. Mag.* **51**, 2505304 (2015).
- [38] A. Hubert and R. Schafer, *Magnetic Domains: The Analysis of Magnetic Microstructures* (Springer, Berlin, 1998).